Identification and Characterization of an Insulin-Like Receptor Involved in Crustacean Reproduction

O. Sharabi, R. Manor, S. Weil, E. D. Aflalo, Y. Lezer, T. Levy, J. Aizen, T. Ventura, P. B. Mather, I. Khalaila, and A. Sagi

Department of Life Sciences (O.S., R.M., S.W., E.D.A., Y.L., T.L., A.S.), The National Institute for Biotechnology in the Negev (S.W., E.D.A., A.S.), and Avram and Stella Goldstein-Goren Department of Biotechnology Engineering (I.K.), Ben-Gurion University of the Negev, Beer-Sheva 84105, Israel; GeneCology Research Centre (J.A., T.V.), Faculty of Science, Health, Education, and Engineering, University of the Sunshine Coast, Maroochydore, Queensland 4558, Australia; and Department of Earth, Environmental, and Biological Sciences (P.B.M.), Science and Engineering Faculty, Queensland University of Technology, Brisbane, Queensland 4000, Australia

Sexual differentiation and maintenance of masculinity in crustaceans has been suggested as being regulated by a single androgenic gland (AG) insulin-like peptide (IAG). However, downstream elements involved in the signaling cascade remain unknown. Here we identified and characterized a gene encoding an insulin-like receptor in the prawn *Macrobrachium rosenbergii* (*Mr-IR*), the first such gene detected in a decapod crustacean. In mining for IRs and other insulin signaling-related genes, we constructed a comprehensive *M. rosenbergii* transcriptomic library from multiple sources. In parallel we sequenced the complete *Mr-IR* cDNA, confirmed in the wide transcriptomic library. *Mr-IR* expression was detected in most tissues in both males and females, including the AG and gonads. To study *Mr-IR* function, we performed long-term RNA interference (RNAi) silencing in young male prawns. Although having no effect on growth, *Mr-IR* silencing advanced the appearance of a male-specific secondary trait. The most noted effects of *Mr-IR* silencing were hypertrophy of the AG and the associated increased production of *Mr-IAG*, with an unusual abundance of immature sperm cells being seen in the distal sperm duct. A ligand blot assay using de novo recombinant Mr-IAG confirmed the existence of a ligand-receptor interaction. Whereas these results suggest a role for Mr-IR in the regulation of the AG, we did not see any sexual shift after silencing of *Mr-IR,* as occurred when the ligand-encoding *Mr-IAG* gene was silenced. This suggests that sexual differentiation in crustaceans involve more than a single Mr-IAG receptor, emphasizing the complexity of sexual differentiation and maintenance. **(*Endocrinology* 157: 928–941, 2016)**

In crustaceans, it is widely accepted that a single peptide hormone factor controls masculine sexual differentiation and its maintenance and that the peptide possesses secondary and tertiary structures resembling those of members of the insulin hormone superfamily (1–3). Accordingly, the peptide was named the insulin-like androgenic gland hormone (IAG). This hormone is produced exclusively by an endocrine gland unique to male crustaceans and referred to as the androgenic gland (AG). Through AG ablation (4, 5) or RNA interference (RNAi)-mediated loss of IAG function, it was shown that this hormone is crucial for sexual differentiation, spermatogenesis, and the appearance of external sexual characteristics, such as the male-specific *appendix masculine* (AM) on the second pair of pleopods (6). Although the androgenic hormone is present in many crustacean species (7), the pathway through which it mediates sexual differentiation, growth, and manifestation of masculine characteristics is poorly understood.

ISSN Print 0013-7227 ISSN Online 1945-7170
Printed in USA

Received May 4, 2015. Accepted December 11, 2015.
First Published Online December 17, 2015

Abbreviations: aa, amino acid; Ab, antibody; AG, androgenic gland; AM, *appendix masculine*; ds, double strand; FN3, fibronectin-3 domains; hAG hypertrophied AG; H&E, hematoxilin and eosin; IAG, insulin-like androgenic gland hormone; ILP, insulin-like peptide; IR, insulin receptor; Mr-IR, *IR* gene in *Macrobrachium rosenbergii*; PL, post larvae; qRT-PCR, quantitative RT-PCR; RB, *Remebee*; rMr-IAG, recombinant Mr-IAG; RNAi, RNA interference; ROI, region of interest; RTK, receptor tyrosine kinase; SD, sperm duct; SMART, Simple Modular Architecture Research Tool; Sulfo-SMCC, sulfosuccinimidyl 4-(N-maleimidomethyl) cyclohexane-1-carboxylate; TBS, Tris-buffered saline; TBST, TBS with Tween 20; TM, transmembrane; WB, Western blot.

The pivotal protein in any insulin family-based signaling pathway is the insulin receptor (IR) that is responsible for mediating the signal carried by insulin-like peptides (ILPs) from the intercellular to the intracellular environment. IRs, like their ligands, are found in almost every metazoan, from *Porifera* to man (8, 9) and can be found in copy numbers as low as 40 molecules and up to more than 200 000 per cell (10).

IRs belong to the superfamily of tyrosine kinase receptors that all possess an intracellular tyrosine kinase domain that undergoes autophosphorylation at conserved tyrosine residues (most commonly on the three tyrosine residues of the typical sequence motif YETDYY) after ligand stimulation. Such phosphorylation is essential for maximal up-regulation of the catalytic activity of the receptor (11). IRs are structurally well conserved throughout evolution yet also present structural changes in regions not critical for ligand binding or phosphorylation (9). The IR precursor is composed of α- and β-subunits that are linked by disulfide bridges to form an $\alpha\beta$-heterodimer. This heterodimer associates with a second $\alpha\beta$-unit, resulting in the mature and functional $\alpha_2\beta_2$-holoreceptor protein (12). The α-subunit, corresponding to the insulin-binding subunit, is wholly extracellular and is linked to the extracellular portion of the β-subunit as well as to the other α-subunit, via disulfide bridges. The β-subunit comprises an extracellular domain, a transmembrane (TM) domain, and the intracellular kinase domain. IRs are very similar to other growth factor receptors, except for the fact that IR protomers are covalently tethered (13).

The role of the insulin-signaling pathway has been well studied in vertebrates, in which it mainly regulates metabolic activity, cell proliferation, and growth, although a single study has suggested a role for this pathway in sexual development (14). In invertebrates, the role of the insulin pathway is more diverse and includes not only glucose homeostasis but also regulation of growth, longevity, and reproduction (12). Indeed, these effects have been attributed to several different insulin-like hormones. In decapod crustaceans, IAG is the sole ILP widely found thus far, with the exception of a *Drosophila* ILP7 ortholog of unknown function, recently identified in a spiny lobster species (15).

Here we report the complete sequencing of an *IR* gene in the giant freshwater prawn *Macrobrachium rosenbergii* (termed *Mr-IR*) as well as its validation using a new composite transcriptomic library. Ligand-receptor binding was established using a novel recombinant Mr-IAG (rMr-IAG) and through the production of mouse anti-rMr-IAG and Mr-IR polyclonal antibodies. Although the use of RNAi revealed that Mr-IR plays a role in regulating the AG and, consequently, the process of spermiogenesis, the expected sex shift noted when the ligand-encoding gene (*Mr-IAG*) was silenced did not occur when the receptor-encoding gene was silenced. Taken together, the results presented here describe the first IR identified in a decapod crustacean and highlight its role in the IAG masculinization pathway.

Materials and Methods

Animals

M. rosenbergii small males (5–12 g) were collected from the Dor research station (Department of Fisheries and Aquaculture, Israel Ministry of Agriculture and Rural Development, Israel) for *dsMr-IR* gene silencing efficiency experiment. *M. rosenbergii* PL_{16} (postlarvae, 16 days after metamorphosis) male offspring from a neofemale animal were maintained at Ben-Gurion University of the Negev, as previously described (16). These individuals were used to study the effects of double-strand (ds) *Mr-IR* treatment (see below). Mature male and female progeny from normal females, collected at the Dor Aquaculture Station (Israel Ministry of Agriculture) were used for tissue specificity assessment. To achieve AG hypertrophy, dominant morphotype males, also known as blue claw males, were endocrinologically induced as previously described (6).

Sequencing of the complete *Mr-IR* transcript and its validation

A key word-based search of available libraries (17, 18) prior to the construction of our new composite transcriptomic library (see Supplemental Materials) yielded a short transcript, which was elongated by 3′ and 5′ rapid amplification of cDNA ends (CLONTECH Laboratories), performed according to the manufacturer's guidelines, using cDNA generated from testis-extracted RNA. Once the composite transcriptomic library had been developed, the above-mentioned sequence served as a reference for read mapping using the CLC Genomic Workbench 7.3 (CLC Bio; default parameters).

Bioinformatic analyses of *Mr-IR* sequence

Once obtained, the complete *Mr-IR* sequence served as a query in a BLAST search designed to reveal homologies between our hypothetical sequence and homologues present in other organisms. To obtain the deduced protein sequence, full length *Mr-IR* cDNA was computationally translated using the ExPASy Proteomics Server (http://ca.expasy.org/tools/dna.html), and the longest open reading frame was selected (ie, the second 5′ to 3′ frame). Conserved domains were identified in the putative Mr-IR protein using the Simple Modular Architecture Research Tool (SMART) (http://smart.embl-heidelberg.de/) (19). Clustal Omega (http://www.ebi.ac.uk/Tools/msa/clustalo/) (20, 21) was then used for multiple sequence alignment of the predicted Mr-IR sequence against those from three representative arthropod members of the IR family, namely from *Daphnia pulex* (GenBank number EFX63421.1), *Aedes aegypti* (GenBank number AAB17094.1), and *Bombyx mori* (NP_001037011), and two representative vertebrates, namely *Homo sapiens* (UniProtKB/Swiss-Prot: P06213.4) and *Mus musculus* (GenBank number AAA39318.1). Sites of N-glycosylation were predicted by the NetNGlyc1.0 server (http://www.cbs.dtu.dk/services/NetNGlyc/).

In silico temporal expression

Sequence reads from male larvae, female larvae, male post larvae (PLs), and female PLs (17) were mapped to the *Mr-IR* reference sequence using STAR (version STAR-2.3.0) (22), using the default parameters. The numbers of IR-mapped reads per sample (ie, male larvae, female larvae, male PLs, and female PLs) were normalized by reads per kilobase of transcript per million mapped reads upon dividing the number relevant reads by the total number of reads recorded from the same sample, multiplied by 1×10^6.

Spatial expression pattern of *Mr-IR*

The spatial expression pattern of *Mr-IR* was examined with RT-PCR. Total RNA was isolated from the testis, AG, hepatopancreas, thoracic-ganglia, head ganglia, green gland, heart, abdomen muscle, and eye stalk from a mature male and from the ovary, hepatopancreas, thoracic-ganglia, head ganglia, green gland, heart, abdomen muscle, and eye stalk from a mature female, as described previously (16). First-strand cDNA was synthesized by reverse transcription using the qScript cDNA kit (Quanta BioSciences) with 1 μg of total RNA. Specific *Mr-IR* forward (5′-AACCAACTTCGTGGCAAAAC-3′, nt 459–479) and reverse (5′-GGTGGAGCAAACCTTGTTGT-3′, nt 1470–1490) primers (see Supplemental Figure 1) were used for PCR amplification, as previously described (16), except that 37 cycles were performed with an annealing temperature of 60°C. *Mr-actin* served as a positive control and was amplified as described previously (6). PCR products were separated and visualized also as described previously (6).

Mr-IR silencing

*ds*RNA *production and silencing efficiency experiment*

Two PCR products were generated using a T7 promoter anchor (T7P; 5′-TAATACGACTCACTATAGGG-3′) attached to one of the two primers used to amplify each product. The primers used for generating the template for sense-strand RNA synthesis were (5′-T7P-ATACCTGCGTTGCTTCCTGT-3′, nt 1605–1625) as forward primer and (5′-GAAGAAGAAGGTGCCGTTGT-3′, nt 2091–2111) as reverse primer. Primers used for generating the template for antisense strand RNA synthesis were (5′-ATACCTGCGTTGCTTCCTGT-3′, nt 1605–1625) as forward primer and (5′-T7P-GAAGAAGAAGGTGCCGTTGT-3′, nt 2091–2111) as reverse primer (See Supplemental Figure 1). PCR amplicons were separated and visualized as described (23). ds*RNA* was prepared, hybridized, quantified, and maintained as described previously (23). For evaluating gene silencing efficiency, small males were divided into three groups. Two groups were endocrinologically induced as previously described (24). The above-mentioned groups were injected three times over a period of 1 week, with ds*Mr-IR* or ds*GFP* (n = 8 and n = 10, respectively). Another control group consisted of untreated individuals (n = 8). Evaluation of *Mr-IR* silencing was done using quantitative RT-PCR (qRT-PCR) as described below (Supplemental Figure 2).

In vivo Mr-IR *silencing*

One hundred thirty-three PL, 16 days after metamorphosis, male individuals, progeny from a neofemale (25), were collected and divided into two groups. Each individual was injected on a weekly basis. Eighty-three individuals were injected with ds*Mr-IR* (5 μg/g body weight). Fifty individuals comprising a control group, were injected with an exogenous dsRNA (ds*Remebee* [RB], a dsRNA formulated to silence Israeli acute paralysis virus affecting bees) (26). The ds*RB* sequence was chosen due to the fact that it does not align to any *M. rosenbergii* mRNA sequences in our composite library. As such, it has been regularly used as a control in our laboratory (16, 23, 27).

Growth rates were documented weekly from the ninth week of the experiment, as was the presence of the AM, a secondary masculine trait, corresponding to an appendage found solely on the second pleopods in male *M. rosenbergii*. This secondary sex characteristic serves to distinguish between male and female individuals at an early age (4). Its development is highly dependent on the size and weight of an individual, which are affected by environmental conditions such as stocking density (28–30). Under conditions similar to the present study, the AM develops in males between 80 and 220 days after metamorphosis (16, 23).

General histology and immunohistochemistry

At the end of the experimental period, representative juvenile prawns (278–2710 mg) were collected and fixed with 4% buffered formalin for 24 hours, followed by dehydration using increasing ethanol concentrations. Samples were then cleared and embedded in Paraplast (Kendall). Dorsoventral sections were cut from the cephalothorax of small animals (278–324 mg). Animals weighing 1725–2710 mg provided sections from the distal part of the sperm duct (SD) found at the base of the fifth walking leg. For immunohistochemistry, consecutive sections of the distal part of the SD were incubated with anti-Mr-IAG antibodies (Ab). Slides were treated as described (6), with a slight modification to the anti-Mr-IAG Ab concentration used (1:250) and viewed by fluorescence microscopy. Nuclear counterstaining was performed using Hoechst dye 33342 (1:1000) (stock solution 16.2 mM) obtained from Invitrogen. To assess histological morphology, representative sections were stained with hematoxilin and eosin (H&E).

For signal intensity assessment, sections were taken from the AG of either ds*Mr-IR*-silenced or untreated animals. In each section four randomly selected regions of interest (ROI) were measured for signal intensity (0–4096 bits) in both Hoechst and Cy3 for Mr-IR labeling or Hoechst and fluorescein isothiocyanate for Mr-IAG labeling, using Olympus Fluoview version 2.1 software. The signal in each ROI was divided by the number of nuclei in that ROI. A *t* test was used to test for difference in signal intensity between treatment and control.

Sperm cell counts

Three sections representing consecutive 250-μm steps along the SD of ds*Mr-IR*-injected and control individuals were stained with H&E. In each section, three random ROIs, sized 100×100 μm each, were selected (yielding a total of nine ROIs per experimental group), and spermatozoa and secondary spermatocytes within ROI were counted using ImageJ 1.48v software (National Institutes of Health, Bethesda, Maryland). A split-plot ANOVA, with treatment and section location as whole-plot treatments, as well as cell type as the within-plot treatment, was used to test for differences in the number of secondary spermatocyte and spermatozoa cells along sperm ducts subjected to the different treatments (ie, ds*IR*-injected vs control).

Relative quantitation of *Mr-IR* and *Mr-IAG* expression levels

For the ds*Mr-IR* silencing efficiency experiment, RNA was extracted from AGs of small males. For the long-term *Mr-IR* in vivo silencing experiment, RNA was extracted from the base of the fifth walking leg of silenced individuals after 22 injections of ds*Mr-IR* and from control individuals injected with ds*RB*. Total RNA isolation, first-strand cDNA synthesis and qRT-PCR were performed as described (23). The relative quantification of *Mr-IR* transcript levels was achieved using the *Mr-IR* qRT-PCR forward (5′-AGCAGCAGCAACACTCGAC-3′ nt 2715–2733) and *Mr-IR* qRT-PCR reverse (5′-CTGTGGGACTCCGGTTTG-3′ nt 2769–2786) primers (see Supplemental Figure 1). *Mr-IAG* transcript levels was achieved using the *Mr-IAG* qRT-PCR forward (5′-GCCTTGCAGTCATCCTTGA-3′) and *Mr-IAG* qRT-PCR reverse (5′-AGGCCGGAGAGAAGAATGTT-3′) primers. For both *Mr-IR* and *Mr-IAG*, probe 144 (Universal Probe library, Rox; Roche Diagnostics) was used. *Mr-18S* (GenBank accession number GQ131934), serving as a normalizing gene, was also quantified by means of qRT-PCR as previously described (23).

rMr-IAG and anti-Mr IAG and anti-Mr IR antibodies production

Using the methylotrophic yeast *Pichia pastoris*, rMr-IAG was produced as a biologically active, single-chain polypeptide according to another report (31), using the Pichia expression kit (Thermo Fisher Scientific). Briefly, DNA encoding the α- and β-chains that comprise the mature Mr-IAG (GenBank accession number ACJ38227.1) were joined to form a fusion gene encoding a tethered polypeptide in which the β-chain forms the N-terminal portion and the α-chain forms the C-terminal portion of the protein. DNA encoding a linker sequence (GSGSHHHHHHHHGSGS) was placed between the α- and the β-chains to assist in chimerization of the subunits, with the His_6 sequence found in the middle of the linker serving to enable purification of the recombinant protein using NiNTA resin (QIAGEN).

Based on the sequences deduced for Mr-IAG and Mr-IR, custom peptides were constructed (Genscript) and used to generate two separate polyclonal antibody preparations in BALB/cOlaHsd mice. Specifically, polyclonal anti-Mr-IAG antibodies were raised against CNNYINPGPTYVSKE from the β-chain sequence, whereas polyclonal anti-Mr-IR antibodies were developed against a mixture of SPSSKARMPSEPHQ and IASGSLDPSLEEEG peptides, corresponding to deduced Mr-IR protein sequences. For antibody preparation, the peptides were reconstituted with miliQ water to a final concentration of 2 mg/mL each (Table 1). Mice were then injected with 200 μL of immunization emulsion containing 25 μg of peptide in PBS, mixed at a 1:1 ratio with Freund's complete adjuvant (Sigma). Thereafter, the mice were boosted at 10-day intervals with immunization emulsion containing 25 μg of either the Mr-IAG peptide or the Mr-IR peptide mix and incomplete Freund's adjuvant (Sigma). Antibody preparation was terminated by mouse heart puncture and maximal blood collection after 40 days. Serum was separated from blood cells by centrifugation at 3000 $\times$ *g* for 10 minutes at 40°C and stored in aliquots at −80°C. Validation of the specificities of the polyclonal antimouse antibodies for peptides specifically chosen from the predicted proteins was performed by Western blot (WB). Because the peptides were too small for examination by SDS-PAGE, each was instead conjugated to BSA using sulfosuccinimidyl 4-(N-maleimidomethyl) cyclohexane-1-carboxylate (Sulfo-SMCC; Thermo Scientific) a cross-linker, with a spacer arm of 8.3 Å, following the manufacturer's instructions. The conjugated proteins tested for anti-Mr-IAG and anti-Mr-IR antibodies validation were prepared using those peptides used for antibody generation (see above).

To further demonstrate the specificity of the mouse anti-Mr-IAG antibodies, a WB was performed using a hypertrophied AG (hAG) homogenate, insulin (I5500; Sigma), and a hepatopancreas homogenate.

Membrane fraction and total protein homogenate preparation

Soluble membrane proteins from homogenized ovary, testis, and hepatopancreas tissues (5 g each) were prepared as described previously (32). A total hAG protein homogenate was prepared in Tris-buffered saline (TBS) containing 0.1% Tween 20 (TBST) and 1 mM protease inhibitor (p7626; Sigma).

WB and ligand blotting

For WB and ligand blot analyses, proteins isolated from various tissues were separated using NuPAGE Novex 4%–12% gradient gels under nonreducing conditions in Tris-3[N-morholino]propanesulfonic acid running buffer, as described by the manufacturer (Invitrogen) and transferred to a nitrocellulose membrane. After blocking with 3% skim milk in TBS, membranes were incubated overnight (4°C) with anti-Mr-IR or anti-Mr-IAG antibodies, at a dilution of 1:750 (vol/vol). After washing three times with TBST, the membranes were incubated with horseradish peroxidase-conjugated goat antimouse antibodies (1:15 000). Antibody binding was detected using FemtoGlow

Table 1. Antibody Table

Peptide/Protein Target	Antigen Sequence (If Known)	Name of Antibody	Manufacturer, Catalog Number, and/or Name of Individual Providing the Antibody	Species Raised (Monoclonal or Polyclonal)	Dilution Used	DOI or Publication Data
Mr-IAG	aa 28-173	Recombinant pro-Mr-IAG	Amir Sagi Lab, Ben-Gurion University	Rabbit, polyclonal	1:750	10.5402/2011/476283
Mr-IAG	CNNYINPGPTYVSKE	rMr-IAG	Amir Sagi Lab, Ben-Gurion University	Mouse, polyclonal	1:750	Endocrinology
Mr-IR	SPSSKARMPSEPHQ, IASGSLDPSLEEEG	Mr-IR	Amir Sagi Lab, Ben-Gurion University	Mouse, polyclonal	1:750	Endocrinology

MITTKSSVMSVLNVKASSTRPIGSAAAARPRSNGFVYHHIRLFLLSVTSMVIISCSVPVLGGYSTPKTCK
SVEITGFRRŃDSLPRHLRECQVMEGHLRLQLIEEEEEDFEDEEEIIEFLSFPNLVQVTEYVVIYRISPLR
SLERILPQLSVIRGHELFHGYALVVIGNTYLERLGLDŃVTDILŃGSVRIEKNWILCPGLDNRWEŃITLKS
REAKNVIQNNYIYCIYDPCETDNSCPTEVRPNNKVCSTVGGGCYQGPQCHPECAGGCLRPNDPSACVACR
NYMLRŃNTCVASCDYDQSYYISENKYLCTEŃATCRRDPDGAKDGSSGSVCNRCKDNNCVPNSCKGTTITS
DDLGRRLRGCEYVDGSLIINIAGGWŃVTQQLEENLKNIRŃVTGYIRVSGSNTLFSLNFLKNLEVIEGKEK
KDNLYVLYIMENEHLQELWEGAKKLTVGNŃGTFFFLYŃPSLCRQLIYDLADRSGVARETLYVSNSTNGQT
LPCYDSEMKAEVHPNREVGTVŃVTWKHIYKGNDHRMVIGYYVFYREAPEŃVTLFGNRDACNDEILWNRHF
WEYEKHEGESRTRTEALQGLKPYTRYAVYVMAYYTDQEKTGSRSRILYVETLPTNPSPVWGITRKHRTAY
DLTLEWRSPSRINGNFIHYRITYKKAKEVTHQPELTCNSPSSKARMPSEPHQPPPAPAGKAŃATSSSAK
TQNAVEADMKCCACQDQNQLYSASIKNDRQFKIAFEDYLDNVLYAKIEŃDTKPPPŃATTTRSPTQKKASP
TFGPITTVPPTTEASTQSVLVVTESESIVDTAAEKDLHDDDNWEDGVIFTKDNFYTLTGLCYFTGYEISI
SACNIDQDQNLLCSIPSLYTDKTMADPQVDAITNFEIMLEGDEERWRRTRRRRERQHAEAVAAEAAAATL
DGGGRWGEGEEVAKPESHRTIGKCHANNYNLSLPARVPVTNTSYSSLYGKNLILSWTPPTNPNGKPRYYI
IDVVDTDAGERKDFRPRCISEEEASKNGYTYRLNDLTPGSYŃISIQLRSEGGDGPFTTEMIRIGDPYLVWI
IVGPLVGGVMVGVCIMKFHLWYRKRRLGAVLEERCVVTINRQYGELLGCARCQINDKYIIDPKDLEIAL
DKKLGEGYFGVVYQGVLKEPSGNAKKVAIKDLNKPDKLNEAKCALEEVHHMQDINSHFIVPLVGVMATKP
SIYIVMELMERGDLRTFLLSEEGCTIKPQKMIEMAIEAADGMAYLAAKKLVHRDLAARNCMLDSKLTLKI
GDFGLTRYLANDYYKKRGEAVLPVRWLAPEALELGRYTSRSDVWSYGVLLWEIYTRGLQPYQGYKNQQVH
EKVIAGTLRLEQPAPCPDFMYAIMNQCWRREPKERPTFIQLIRILLPRAVPEYLEFLERVSFFHKSNGCD
SESTEDNDEGFIASGSLDPSLEEEGEEDDEENEDDIEGDHSFSSSIPHSLHNTEDDQVCLTPDEHYNKRM
SCGSLSCINGNPKGVGIRLTPTKDTSYQLLYHKPTSFA

Figure 1. The Mr-IR open reading frame. Deduced amino acid sequence of Mr-IR and predicted N-glycosylation sites. Beginning at the N terminus, one finds a TM domain (bold, double underlined), two ligand-binding domains (bold and italicized, gray background), a furin-like domain (dashed underline), three FN3 domains (italicized, underlined), and a tyrosine kinase domain (gray boxes) and predicted N-glycosylation sites (capital N with accent mark).

WesternPLUS (Michigan Diagnostics). For ligand blotting, membranes and tissue homogenate proteins were separated on nonreducing SDS-PAGE and transferred to a nitrocellulose membrane. After blocking with 3% skim milk in TBS, membranes were incubated overnight in HEPES ligand solution (containing 20 mM HEPES, pH 7.4; 150 mM NaCl; 2 mM $MnCl_2$; 10 mM $MgCl_2$) with 1% skim milk and 1 mg/ml rMr-IAG. The membranes were washed with TBST and incubated with anti-Mr-IAG and goat-antimouse antibodies as above.

Results

Mr-IR transcript and deduced protein sequence

A composite transcriptome library containing more than 290 million reads and expressed sequence tags was assembled into 108 212 contigs. Contig length distribution, filtering and GO analysis are described in the Supplemental Materials section and in Supplemental Figures 3 and 4. A key word-based search of this composite transcriptomic library, as well as a previously generated *M. rosenbergii* transcript library (18), yielded sequence possessing high similarity (as high as 30%) with known IRs in the GenBank database and was therefore named *M. rosenbergii* insulin receptor (*Mr-IR*). *Mr-IR* is 6600 nucleotides long, with a predicted open reading frame encoding a 1508-amino acid (aa) translation product, a 746-bp 5′-untranslated region, and a 1330-bp 3′-untranslated region ending with a poly-A tail (Supplemental Figure 1). Examination of the deduced Mr-IR amino acid sequence identified conserved domains that characterize reported IRs, specifically two TM domains (aa 42–64 and 1050–1072), two ligand-binding domains (aa 89–207; E-value $7.4e^{-19}$, and aa 359–471; E-value $1.7e^{-20}$), three fibronectin-3 domains (FN3; aa 494–601, 616–849, and 946–1034, E-values between 10.377 and $4.49e^{-4}$), and a tyrosine kinase domain (aa 1118–1375; E-value $5.31e^{-131}$) (Figure 1 and Supplemental Figure 1).

Validation of the *Mr-IR* sequence in *M. rosenbergii* composite transcriptomic library

Of the total of 291 214 114 reads and expressed sequence tags found the composite transcriptomic library developed as part of this study (that included *M. rosenbergii* genes found in the National Center for Biotechnology Information online database), 4339 reads (composed of 292 889 bases) with an average length of 67.50 bases each were mapped to the reference *Mr-IR* cDNA. The map of this alignment is shown in Figure 2A. The length distribution of all mapped reads and the length distribution of the total reads in the entire library are shown in Supplemental Figure 5, A and B, respectively. This alignment offered a complete validation of the *Mr-IR* sequence and demonstrated the comprehensiveness of the composite transcriptomic library compared with previous libraries.

Bioinformatics analysis of Mr-IR

SMART representations of Mr-IR and the complete sequences of phylogenetically related IRs from *D. pulex*,

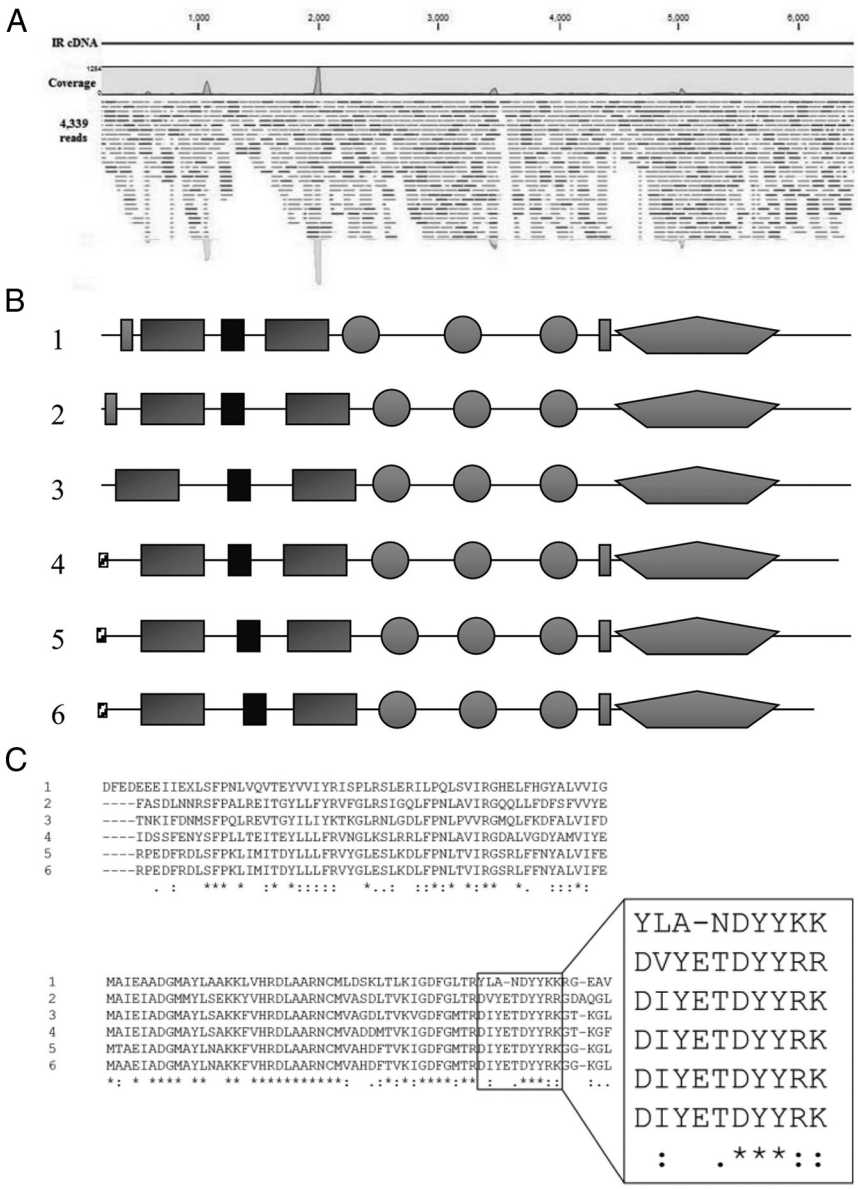

Figure 2. Mr-IR sequence analysis. A, Alignment of reads from the wide transcriptomic library mapped to the *M. rosenbergii IR* cDNA. The light gray lines represent forward reads, whereas the dark gray lines represent reverse reads. The long black line above the reads defines the reference *Mr-IR* cDNA comprising 6600 bases. The coverage graph along the sequence is also displayed. B, SMART algorithm representation of predicted IR domains in Mr-IR and in representative invertebrate and vertebrate IR proteins. Domains are represented as follows: signal peptide (striped rectangle), ligand-binding domains (dark gray rectangles), furin-like domain (black rectangle), FN3 domains (circles), TM domains (light gray rectangles), and a tyrosine kinase domain (pentagon). Numeric representation of the species are as follows: 1, *M. rosenbergii*; 2, *D. pulex*; 3, *B. mori*; 4, *A. aegypti*; 5, *M. musculus*; 6, *H. sapiens*. C, Multiple sequence alignment of the first Mr-IR ligand-binding domain (top) and part of the tyrosine kinase domain (bottom) of three representative invertebrate and two vertebrate insulin-related receptors. Numbers represent species as indicated above. *, Fully conserved residues; :, residues with strongly similar properties; ., residues with weakly similar properties.

a cladocera crustacean, *B. mori*, and *A. aegypti* (arthropods) and the distant *M. musculus* and *H. sapiens* (vertebrates) demonstrated that IR domain composition and organization are conserved from *Crustacea* to mammals. Starting from the N-terminal end of the putative sequence, one finds a TM (Figure 2B, light gray *M. rosenbergii* and *D. pulex*) or a signal peptide (Figure 2B. stripes, *A. aegypti*, *M. musculus*, and *H. sapiens*) followed by two ligand-binding domains (Figure 2B, dark gray), separated by a furin-like domain (Figure 2B, black). After the ligand binding domains, one finds three FN3 domains (Figure 2B, circles), a TM domain, and finally, a tyrosine kinase domain (Figure 2B, pentagon) at the C-terminal end. Multiple sequence alignment of the first ligand-binding domain and part of the tyrosine kinase domain in Mr-IR with those from IRs from the taxa listed above, computed using the Clustal Omega algorithm, revealed a high degree of similarity (Figure 2C). The sequence YETDYY is the highly conserved auto-phophorylation sequence motif of the IR tyrosine kinase domain (33). In Mr-IR, this autophosphorylation sequence deviates from the consensus sequence by substitution and insertion of the amino acids sequence LAND (Figure 2C, top line in magnified box).

A search for predicted N-glycosylation sites in the putative Mr-IR protein sequence revealed 17 sites containing the sequence motif, NXS/T (in which X is any amino acid except proline) in the ectodomain.

Spatial and temporal *Mr-IR* expression patterns

RT-PCR showed that in adult *M. rosenbergii*, the *Mr-IR* transcript was expressed in gonads, heart, thoracic ganglia, head ganglia, green gland, and eye stalk in both male and female individuals (Figure 3, arrow). Amplification was also observed in the AG. No expression was detected in muscle or hepatopancreatic tissue in either sex. (Figure 3A shows results from a representative male and female in the intermolt stage). The same expression pattern was observed in several replicates. Reads mapped to *Mr-IR* were found in all four groups of our larval and PL transcriptomic library (17), albeit in only relatively low numbers (Figure 3B).

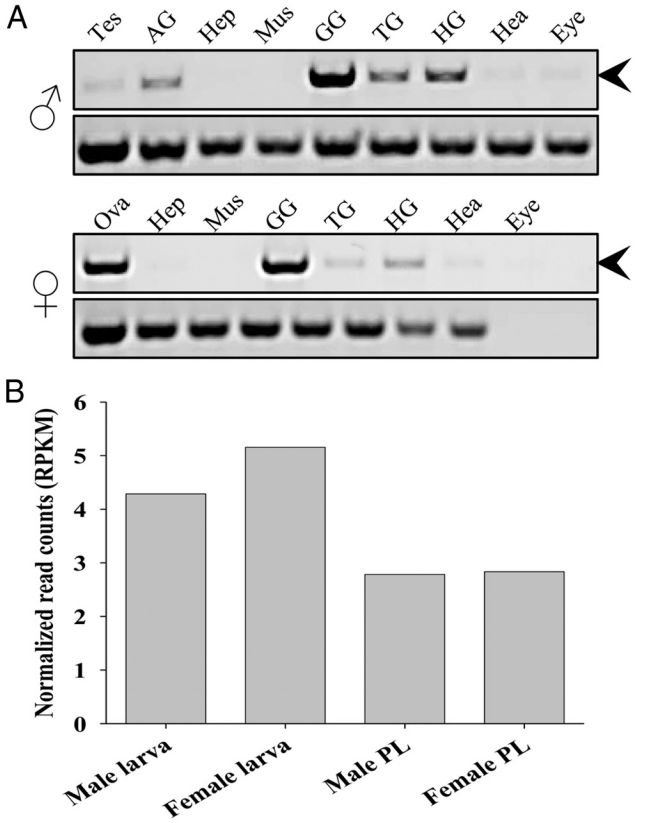

Figure 3. *Mr-IR* expression patterns. A, Spatial expression in various mature *M. rosenbergii* male and female tissues. *Mr-IR* cDNA expression was shown by RT-PCR (top panel). cDNA for *M. rosenbergii β-actin* (bottom panel) served as a positive control. AG, androgenic gland; GG, green gland; Hea, heart; Hep, hepatopancreas; HG, head ganglia; Mus, muscle; Tes, testis; TG, thoracic ganglia. B, In silico *Mr-IR* temporal expression in young *M. rosenbergii* stages. The number of mapped reads per sample (ie, male larvae, female larvae, male PLs, and female PLs) was normalized by reads per kilobase of transcript per million mapped reads (RPKM), dividing it by the total number of reads from that sample and multiplied by 1×10^6.

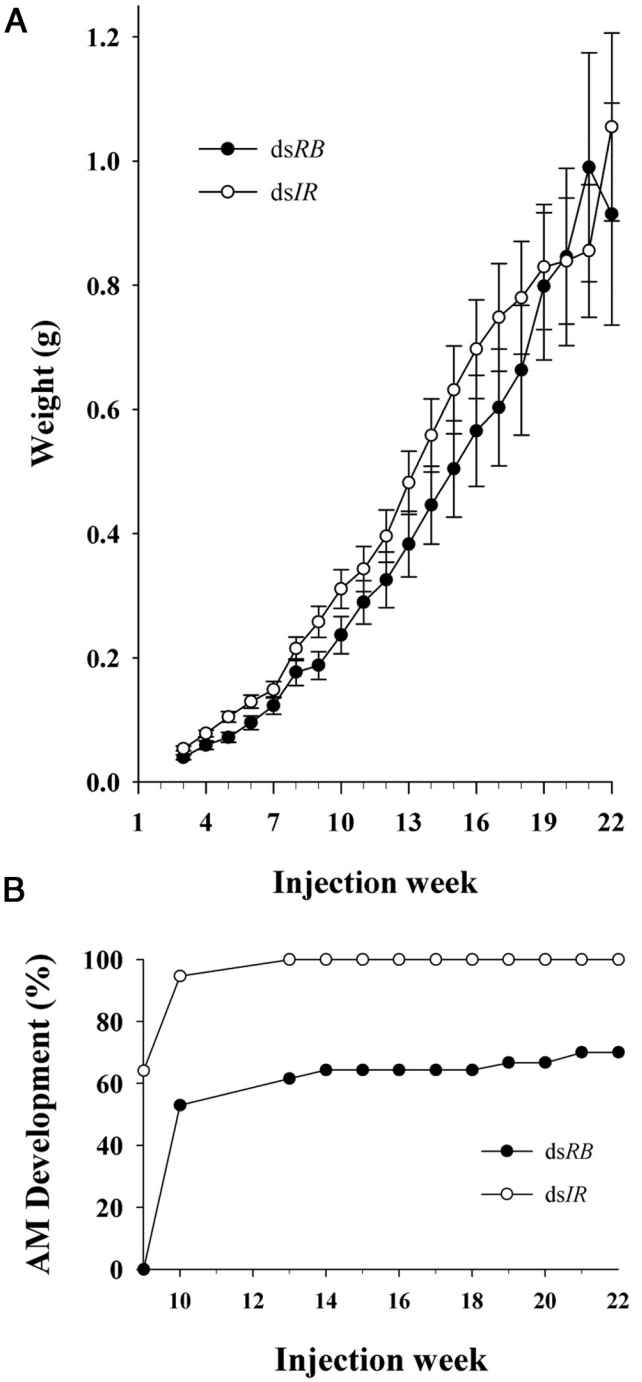

Figure 4. Growth and sex characteristics in *Mr-IR*-silenced vs control PL animals. A, Effects of *Mr-IR* dsRNA injection on growth. Average body weight of *Mr-IR*-dsRNA-injected (○) and ds*RB*-injected (●) groups. Weekly injections started 20 days after metamorphosis (two way ANOVA, $P < .05$). B, Male secondary sexual trait appearance. Fraction (percentage) of *Mr-IR*-dsRNA-injected (○) and ds*RB*-injected (●) individuals that have developed an AM during the injection period.

Mr-IR silencing and its effects

Mr-IR silencing resulted in several phenotypic and physiological abnormalities. Whereas somatic growth was not significantly different between the treatment and control groups (Figure 4A; two-way ANOVA, $P < .05$), most individuals in the treatment group developed an AM, a secondary masculine trait, earlier than did members of the control group. By the ninth injection, 66% of the injected group individuals at PL_{80} had already developed an AM while in the control group no AM was observed in any individual at this point (Figure 4B). At week 13 of the experiment (ie, at PL_{105}) 100% of the treatment and 64% of the control group possessed an AM, with these levels remaining stable through to week 22.

A day after the final injection (wk 22, PL_{182}), animals were dissected for histology. H&E-stained sperm duct sections showed different ratios between spermatozoa (black arrows) and secondary spermatocytes (white arrows) in ds*IR*-injected vs control animals (Figure 5A). When secondary spermatocytes and spermatozoa were counted in sperm ducts of ds*IR*-injected and control animals, differences in the numbers of the two cell types were not consistent between the two treatments (treatment × cell type

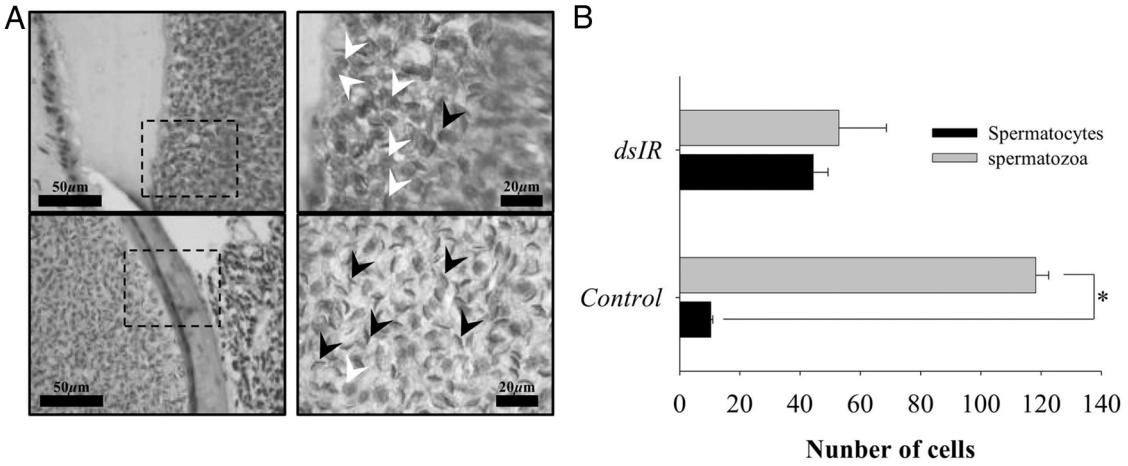

Figure 5. *Mr-IR* silencing affects spermiogenesis. A, Spermiogenesis. Cross-sections from the base of the fifth pereiopod of ds*Mr-IR*-injected (top) and untreated animals (bottom). Black arrows, mature spermatozoon; white arrows, secondary spermatocyte. B, Cell type quantification. For each treatment, two types of cells were counted in nine randomly selected cross-sections. In each cross-section, mature and immature cells were counted in three randomly selected ROIs. Asterisks represent the statistically significant difference observed between the number of cell types in the control SD (paired *t* test, $P < .001$).

interaction; $F1,12 = 442.055$, $P < .001$) (Figure 5B). Specifically, in the control group, the number of secondary spermatocytes was significantly lower than the number of spermatozoa cells, yet no such differences were detected in the ds*IR* treatment group (Figure 5B). Furthermore, this pattern did not vary significantly along the sperm duct ($F2,12 = 3.1$, $P < .083$). More than 4 times the number of secondary spermatocytes were found in the sperm ducts of ds*IR*-injected animal (44% of the counted cells) (Figure 5A, top panel, white arrows; Figure 5B, top panel), as compared with the numbers counted in control animals (10% of the counted cells) (Figure 5A, bottom panel, black arrows, Figure 5B, bottom panel). The AGs of individuals from the treatment group appeared to have hypertrophied and were hyperplasic (Figure 6, top panel, and Figure 7A, II). They were, moreover, at least 3 times larger than the AGs from control individuals (Figure 6, III and VI, and Figure 7, I and II). Treatment group individuals also possessed sperm ducts of a larger diameter that had thinner muscle layers (Figure 6, II), again as compared with the control group (Figure 6, V).

Immunohistochemistry of AGs from treatment, control, and hAGs, using anti-Mr-IAG antibodies (green fluorescence), showed that the hypertrophied AG from the treatment group appeared to possess 10 times more florescence signal of Mr-IAG than the control AGs (*t* test, $P < .001$; Figure 7C) but not as much as endocrine-induced hypertrophied AGs. This difference was evident in lower intensity of green fluorescence in the control (Figure 7A, IV) and the higher intensity in the endocrine induced hypertrophic AG (Figure 7A, VI). Hypertrophy was also detected upon Hoechst staining of DNA, marking the nuclei of the AG cells. In the control gland, nuclei appeared crowded, whereas in the *Mr-IR*-silenced AGs, nuclei were dispersed, as was also true for endocrine-induced AGs. This indicates that cells were swollen, as was also evident in the H&E sections (Figure 6, III and VI) and immune-stained sections (Figure 7A, I-III). The normalized signal intensity of anti-Mr-IR antibodies in treated sections was reduced by 1.6 (paired *t* test $P < .01$) compared with the signal intensity of control sections (Figure 7B, I and II, and Figure 7C).

Real-time RT-PCR performed using RNA extracted from the base of the fifth walking legs, in which the AG is located, showed a significant, 3 orders of magnitude increase in *Mr-IAG* transcript levels in *Mr-IR*-silenced males, as compared with the control group (Mann-Whitney *U* test, $P < .001$; Figure 7D).

Validation of anti-Mr-IAG and anti-Mr-IR antibodies specificity

The specificities of both polyclonal anti-Mr-IAG and anti-Mr-IR antibodies developed in mouse were demonstrated by WB using BSA-conjugated to the respective peptides as positive controls. Both BSA alone and BSA-SMCC served as negative controls (Figure 8A). The successful conjugation of BSA to the different peptides was demonstrated by a shift of CBB-stained bands (Figure 8A, lanes 3 and 9). The specificities of the anti-Mr-IAG (lane 6) and anti-Mr-IR (lane 12) antibodies were also demonstrated. Abs cross-reacted neither with BSA alone nor with BSA-SMCC (lanes 4 and 5 for anti-Mr-IAG and lanes 10 and 11 for anti-Mr-IR antibodies). The presence of the protein encoded by *Mr-IAG* was revealed by the anti-Mr-IAG antibodies, which recognized a specific band of 17.3 kDa in a total hAG protein homogenate. Additionally, these an-

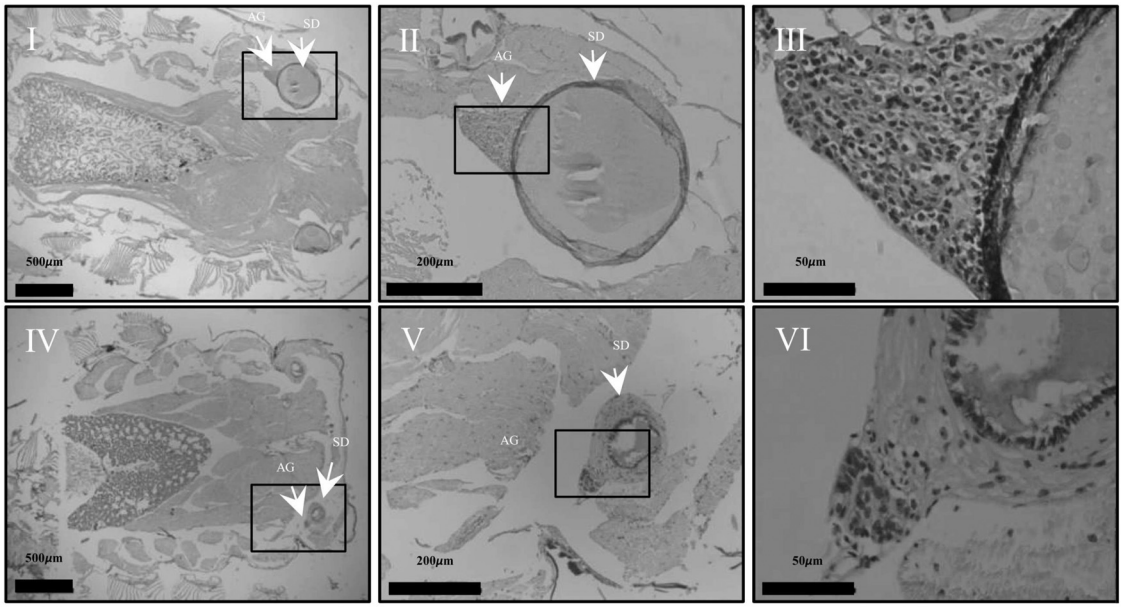

Figure 6. *Mr-IR* silencing induces AG hypertrophy. AG hypertrophy. Shown are dorsoventral sections of a *Mr-IR*-silenced individual (I-III) and a ds*RB*-injected individual (IV–VI). The weight of the *Mr-IR*-silenced individual was 278 mg, whereas that of the ds*RB*-injected control individual was 324 mg.

tibodies also detected the 11-kDa NiNTA-purified rMr-IAG expressed in *P. pastoris* yet did not cross-react either with insulin or with any proteins from the hepatopancreas homogenate (Figure 8B).

Mr-IR and Mr-IAG interaction

The correlation between *Mr-IAG* transcript levels and *Mr-IR* silencing demonstrated above (Figure 7D) suggested a possible ligand-receptor interaction. We therefore conducted WB analysis on proteins isolated from gonads, hepatopancreas, and an AG homogenate using Mr-IR polyclonal mouse antibodies. Under nonreducing conditions, the anti-Mr-IR antibodies cross-reacted with three high-molecular-weight proteins approximately 300–400 kDa in size present in the total AG homogenate (Figure 8C-1). A similar pattern was also observed upon such analysis of a testis homogenate and in purified ovarian membranes, although at different concentrations (Supplemental Figure 6). To test receptor-ligand binding capacity, an identical membrane was prepared under the same conditions as used for the WB. This time, however, the membrane was initially incubated with the recombinant ligand, rMr-IAG. Thereafter, anti-Mr-IAG antibodies were used to assess whether the bait rMr-IAG interacted with the prey Mr-IR protein found on the membrane. Three predominant bands approximately 300–400 kDa in size were observed in the ligand-receptor interaction, identical in position to those bands that cross-reacted with the anti-Mr-IR antibodies (Figure 8, C1 and C2). This indicated that the bait protein was bound to the membrane in which prey proteins were located, confirming a specific interaction between the two. The pattern observed above and high-molecular-weight proteins were completely absent when identical membranes were subjected to WB alone using anti-Mr-IAG antibodies (ie, without incubation with the ligand; Figure 8C-3).

Discussion

The insulin signaling pathway is one of the most studied pathways in higher animal taxa and is involved in many key aspects of life (12), ranging from metabolism to development (34) and longevity (35). In crustaceans, ILPs identified to date are involved in key regulatory processes including sexual differentiation and maintenance of sexual characteristics (36). This is indeed, the case for IAGs. However, apart from characterization of the hormone itself, little information regarding other elements of the signal transduction pathway involving IAGs is available.

IRs are pivotal players in signaling pathways, which mediate insulin and ILP signaling. Such IRs possess a highly conserved tyrosine kinase domain and receptors that belong to the tyrosine kinases super family of receptors (receptor tyrosine kinase [RTK]) (37). Despite their importance, insulin-like receptors have been described to date in only one crustacean species, *D. pulex*. In scanning the composite transcriptome library developed in the present study and previous libraries available for the decapod *M. rosenbergii* (17), we found several contigs that were used to assemble *Mr-IR* (Figures 1 and 2). Whereas the putative *D. pulex* IR sequence is the first to be identified

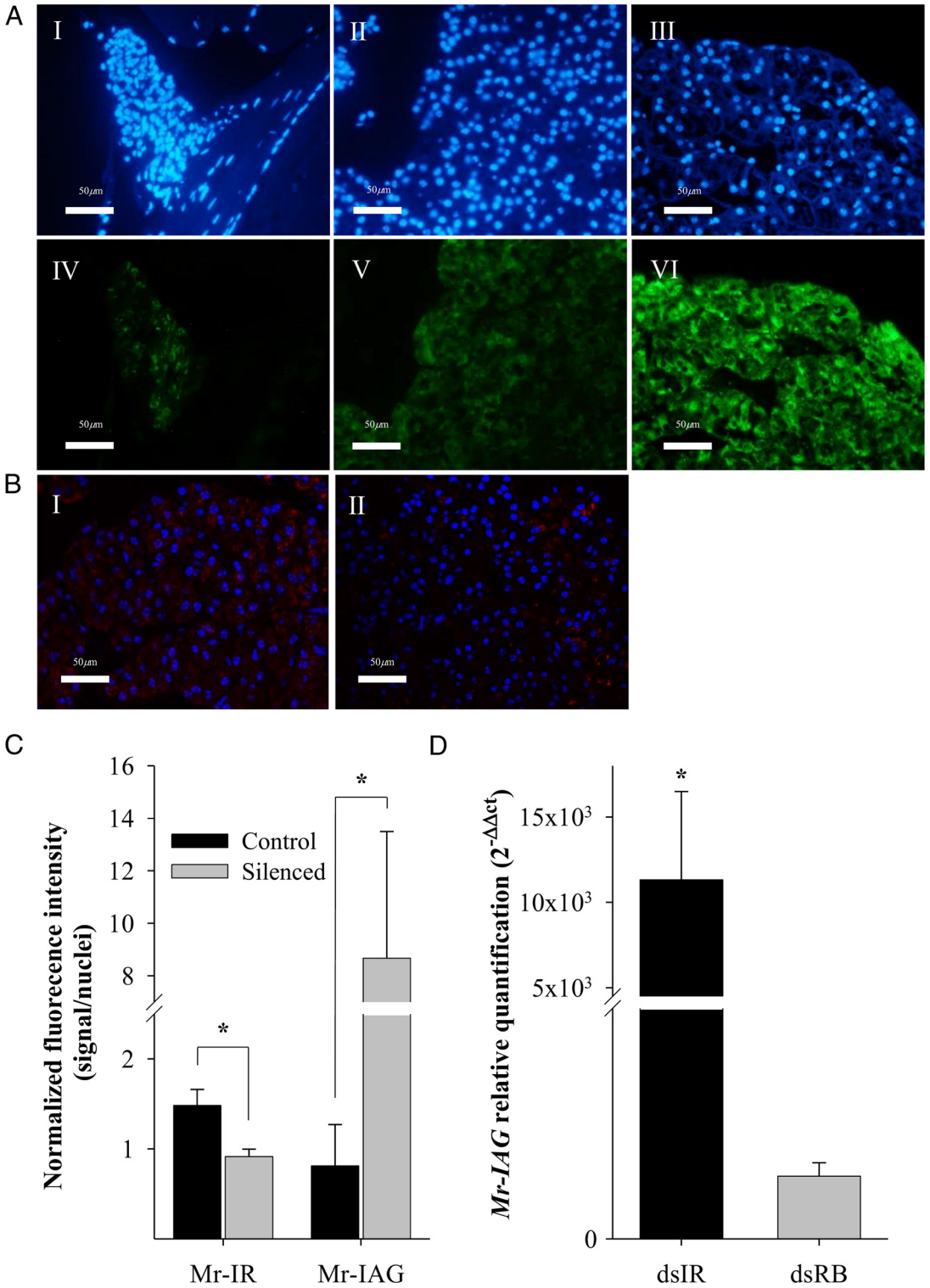

Figure 7. *Mr-IR* silencing effect over AG products. A, Relative abundance of Mr-IAG in AGs from untreated, endocrinologically induced, or ds*Mr-IR*-injected prawns. Immunohistochemistry was performed on cross-sections from the base of the fifth pereiopod of untreated (I and IV), induced (III and VI), and *Mr-IR* dsRNA-injected (II and V) individuals. Mr-IAG presence and abundance are reflected in the green fluorescence of bound goat antirabbit fluorescein isothiocyanate-conjugated antibodies (IV-VI). Hoechst counterstain was used to identify nuclei (I-III). Bar, 50 μm. B, Relative abundance of Mr-IR in AGs from untreated and ds*Mr-IR*-injected prawns. Immunohistochemistry was performed on cross-sections of untreated (I) and *Mr-IR* dsRNA-injected (II) individuals. C, Normalized signal intensity (signal/nuclei) of Mr-IAG and Mr-IR in control and treated AG sections. D, *Mr-IAG* transcript levels. Transcript levels of *Mr-IAG* in AGs from ds*Mr-IR*-injected (black) and ds*RB*-injected control (gray) were measured using real-time RT-PCR. Asterisks represent statistically significant differences (Mann-Whitney *U* test, $P < .01$).

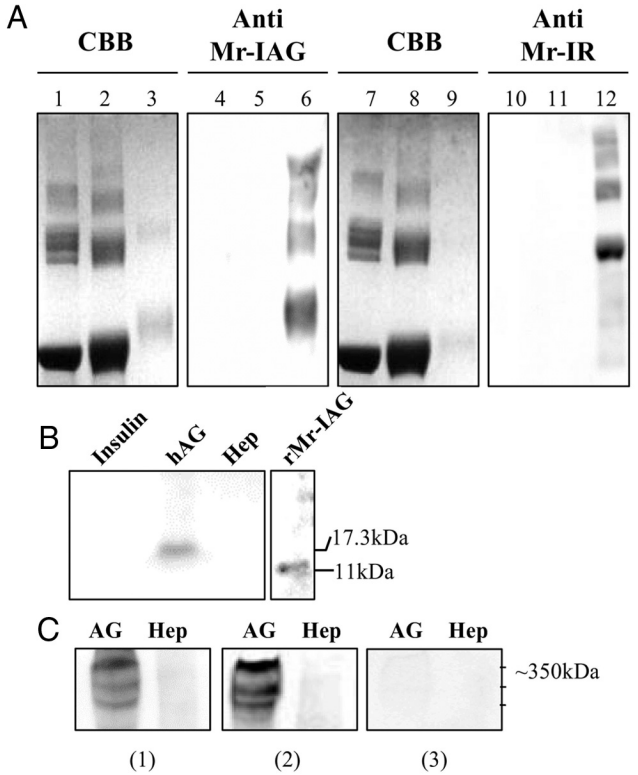

Figure 8. Mr-IAG cross-reacts with Mr-IR. A, The specificities of anti-Mr-IAG and anti-Mr-IR antibodies to peptides cross-linked to BSA via Sulfo-SMCC (lanes 3, 6, 9, and 12) were shown by WB. BSA (lanes 1, 4, 7, and 10) and BSA-Sulfo-SMCC (lanes 2, 5, 8, and 11) served as negative controls for the specificities of both antibodies. The weight shift of BSA cross-linked to peptides was demonstrated using Coomassie brilliant blue (CBB) staining. B, Immunodetection of Mr-IAG by WB. The black arrow indicates pro-Mr-IAG in the hAG extract (17.3 kDa). The open arrow indicates recombinant Mr-IAG (~11 kDa). Hepato, hepatopancreas, C, 1, Immunodetection of Mr-IR by WB in a total androgenic gland protein homogenate (immunoreactive proteins are indicated by arrows); 2, a similar membrane was incubated overnight with rMr-IAG and immunoblotted with anti-Mr-IAG serum; 3, a negative control WB was incubated with anti rMr-IAG antibodies alone.

in crustaceans, Mr-IR is the first IR reported in the important decapod group and the first to be functionally studied in any crustacean species.

For many years, description of the transcriptome was dependent on Sanger sequencing technology that can only provide information regarding the most abundant transcripts, thereby providing only a partial and potentially biased picture (38). Next-generation sequencing platforms, also known as RNA sequencing, have enabled in-depth RNA analysis via cDNA sequencing on a massive scale (39). In the present study, we aimed to identify and characterize genes related to the insulin-like cascade, and more specifically, the gene encoding the receptor mediating Mr-IAG effects, using transcriptomic libraries. Unlike previous libraries (17, 18), the new transcriptomic library reported here revealed a comprehensive coverage of the novel IR. To the best of our knowledge, our composite transcriptomic library for *M. rosenbergii* is the largest available for the species to date and will permit additional mining for insulin-like signaling pathway-related genes in crustaceans.

Alignment of the putative Mr-IR amino acid sequence with those of IRs from other invertebrate and vertebrate taxa showed similar domain composition and organization, with only slight differences. Although for most known IRs cDNAs start with a signal peptide, there are some insulin-like receptors that instead begin with a TM domain, as found here for Mr-IR and as recorded with the *D. pulex* IR (40) and several other invertebrate insulin receptors including those of *Drosophila sechellia* (GenBank accession number EDW55310.1), *D. yakuba* (Genbank accession number XP_002096576.1), *Trichinella spiralis* (EFV59569.1), and others. The function of such a domain at the start of the putative protein sequence remains, however, unknown (40). Not surprisingly, of all the receptor domains identified, the highest sequence similarity was evident for the tyrosine kinase domain, corresponding to the catalytic domain of the receptor responsible for phosphorylating second-messenger proteins inside the cell and thus mediating ILP signaling in target cells (12). IRs and IGF receptors share a highly conserved sequence in the regulatory loop with a typical motif that includes the peptide sequence YETDYY (33). Phosphorylation of the three tyrosine residues in this motif is essential for the up-regulation of receptor catalytic activity. In contrast, the putative tyrosine kinase sequence motif YLANDYY found in Mr-IR in the present study deviates from the conserved YETDYY motif. Further studies will be required to determine whether this difference affects autophosphorylation and, if so, to define the physiological significance of this change. Given, however, the strong sequence conservation shared by IRs, even among lower invertebrates (12), we cannot rule out that an additional insulin-like receptor carrying the YETDYY motif in its tyrosine kinase domain is present in the prawn, in particular when we consider that more than a single IR was identified in the water flea *D. pulex* (40).

Glycosylation is a common and highly diverse co- and posttranslational protein modification. Indeed, almost all proteins present in animal cell membranes are glycosylated, and the notion that almost half of all proteins are glycoproteins are now widely accepted (42). Protein glycosylation serves a diverse array of roles including provision of ligand-binding specificity and protein conformation and stability (43). The human IR is heavily glycosylated and is estimated to contain 58–64 kDa of carbohydrate. It contains 18 potential sites for N-linked glycosylation, of which 16 have been confirmed (44). In

comparison, the novel Mr-IR identified here presents 17 predicted N-glycosylation sites on its ectodomain, as compared with human IR, further supporting our assumption that Mr-IR is an insulin-like membrane-bound receptor. If so, this carries significant implications for the early evolutionary development of IRs.

The insulin signaling pathway is known to play a role in growth regulation (45), neural development (46), differentiation (47), and longevity (48). The first hint for early *Mr-IR* expression in larval stages came from our next-generation sequencing transcriptome library and was validated in vitro. *Mr-IR* is expressed in a variety of tissues in adult male and female *M. rosenbergii* (Figure 3). However, unlike what occurs in vertebrates, *Mr-IR* was not expressed in muscle tissue, implying that Mr-IR does not take part in somatic cell proliferation, an involvement seen in other study organisms including *D. melanogaster* (49) and *Hydra vulgaris* (50). Moreover, unlike the silencing of *Mr-IAG* that produced a negative effect on growth rate, as did silencing of *Mr-EGFR*, another RTK (6, 23), silencing of *Mr-IR* did not affect growth in the present study (Figure 4A).

Ventura et al (6, 16) showed that silencing of the insulin-like hormone in adult *M. rosenbergii* males resulted in partial feminization, and indeed, when silencing occurred at an appropriately early developmental stage, complete sex reversal was obtained. We hypothesized therefore that silencing expression of a receptor for Mr-IAG would yield similar results to those. Yet in the present study, no morphological shift involving sex reversal was seen either during or after the experiment. The development of the AM is growth rate dependent and thus is affected by environmental conditions such as stocking densities (28, 29) and can vary among individuals from the same progeny and among different progenies. Because both the *Mr-IR*-silenced and control groups addressed here were fed ad libitum, kept at similar densities, and showed similar growth rates (Figure 4A), it was surprising to observe an earlier development of the AM in the *Mr-IR*-silenced group but not in the control ds*RB*-injected group (Figure 4B). The results showed an early development pattern different from a typical pattern described by Ventura et al (16). Moreover, when PL males at similar developmental stages were injected with water or ds*RB* as controls, AM appearance showed a similar tendency as previously described (16, 23), suggesting a causative relationship between *Mr-IR* silencing and early male sexual character development and maturation. It has been reported in other decapod species, notably a shrimp in the *Litopenaeus* clade, that the terminal ampule contains mainly mature spermatozoa (51), as was found in the control group of *M. rosenbergii* males in the present study. In contrast, the unusual content of sperm ducts in the *Mr-IR*-silenced group (Figure 5, A and B), reflected as a high occurrence of secondary spermatocytes, also suggests involvement of Mr-IR in either sperm maturation or regulation of sperm release from the testis into the sperm duct.

In both male and female decapod crustaceans, the X-organ-sinus gland complex in the eyestalk produces neurohormones that regulate major physiological processes. Removal of the X-organ-sinus gland complex by eyestalk ablation leads to hypertrophy and hyperplasia of the AG, which then results in overproduction of IAG (41, 52). Unexpectedly, long-term silencing of *Mr-IR*, confirmed by immunohistochemistry, caused similar cellular effects to those observed after endocrine induction by bilateral eyestalk ablation (53). For Mr-IAG, the result corresponds to the elevation of *Mr-IAG* transcript. This implies that the Mr-IR is somewhat downstream from neuroendocrine factors produced in the eyestalk X-organ-sinus gland complex and controls the reproductive organs in decapod crustaceans as suggested by Khalaila et al (52). Sroyraya et al (53) proposed this endocrine axis to be governed by an inhibitory hormone produced by the sinus gland that controls IAG production. The interaction between the receptor, Mr-IR, and the ligand, Mr-IAG, deduced from the ligand blot assay (Figure 8C) may imply a role for the receptor as part of the sinus gland-AG-gonad axis in the sense that it links the IAG with its target organ. This would position Mr-IR as a candidate receptor for Mr-IAG, thus mediating part of the pleiotropic endocrine affects manifested by Mr-IAG. Mr-IR could also regulate Mr-IAG expression, possibly through cross-talk with eyestalk-borne neuropeptide(s) or potentially via auto/paracrine feedback with the AG itself.

Nef et al (14) demonstrated that XY mice mutants for three insulin-like receptors (ie, IR, IGF-1 receptor, and IR related protein, either separately or in all possible combinations) developed a range of sexual differentiation phenotypes. These ranged from the presence of testis through ovotestis to a complete female phenotype suggesting differential contribution by each receptor. Similar results were observed in prawns after *Mr-IAG* silencing (16). If Mr-IAG is indeed a single ligand mediating sexual differentiation, as suggested by Ventura et al (16) and in light of our findings, it is likely that sexual differentiation, at least in decapod crustaceans, could potentially be mediated via more than a single receptor. This would, motivate us to further explore our data for additional RTKs that bind Mr-IAG. Identification of such hypothetical receptors would further clarify the mechanism behind crustacean sexual differentiation.

Acknowledgments

We thank Ms Ayana Benet-Perlberg and her team at the Dor Research Center, Department of Fisheries and Aquaculture, Israel Ministry of Agriculture and Rural Development, for housing and maintaining the experimental prawns. We thank Dr Vered Chalifa-Caspi and her team from the Bioinformatics Core Facility at The National Institute for Biotechnology in the Negev for their help with bioinformatics analysis. We also thank Professor Ofer Ovadia for his help with the statistical analyses.

Address all correspondence and requests for reprints to: Amir Sagi, PhD, Department of Life Sciences and the National Institute for Biotechnology, Ben-Gurion University of the Negev, PO Box 653, Beer-Sheva 84105, Israel. E-mail: sagia@bgu.ac.il.

This work partially supported by the United States-Israel Binational Agricultural Research and Development Fund Grant IS-4493-12; the Israel Science Foundation and the National Natural Science Foundation of China Grant 605/14; and the Seventh Framework Program of the European Union Grants PEOPLE-2013Marie Curie and PIRSES-GA-2013-612296, DeNuGReC.

Disclosure Summary: The authors have nothing to disclose.

References

1. **Martin G, Sorokine O, Moniatte M, Van Dorsselaer A.** The androgenic hormone of the crustacean isopod *Armadillidium vulgare*. *Ann NY Acad Sci*. 1998;839:111–117.
2. **Ohira T, Hasegawa Y, Tominaga S, Okuno A, Nagasawa H.** Molecular cloning and expression analysis of cDNAs encoding androgenic gland hormone precursors from two porcellionidae species, *Porcellio scaber* and *P dilatatus*. *Zool Sci*. 2003;20(1):75–81.
3. **Manor R, Weil S, Oren S, et al.** Insulin and gender: an insulin-like gene expressed exclusively in the androgenic gland of the male crayfish. *Gen Comp Endocrinol*. 2007;150(2):326–336.
4. **Nagamine C, Knight AW, Maggenti A, Paxman G.** Effects of androgenic gland ablation on male primary and secondary sexual characteristics in the Malaysian prawn, *Macrobrachium rosenbergii* (de Man), with first evidence of induced feminization in a non-hermaphroditic decapod. *Gen Comp Endocrinol*. 1980;41:423–441.
5. **Aflalo ED, Hoang TTT, Nguyen VH, et al.** A novel two-step procedure for mass production of all-male populations of the giant freshwater prawn *Macrobrachium rosenbergii*. *Aquaculture*. 2006; 256(1–4):468–478.
6. **Ventura T, Manor R, Aflalo ED, et al.** Temporal silencing of an androgenic gland-specific insulin-like gene affecting phenotypical gender differences and spermatogenesis. *Endocrinology*. 2009; 150(3):1278–1286.
7. **Huang X, Ye H, Huang H, Yang Y, Gong J.** An insulin-like androgenic gland hormone gene in the mud crab, *Scylla paramamosain*, extensively expressed and involved in the processes of growth and female reproduction. *Gen Comp Endocrinol*. 2014;204:229–238.
8. **Skorokhod A, Gamulin V, Gundacker D, Kavsan V, Muller IM, Muller WEG.** Origin of insulin receptor-like tyrosine kinases in marine sponges. *Biol Bull*. 1999;197(2):198–206.
9. **Muggeo M, Ginsberg BH, Roth J, Neville DM Jr, De Meyts P, Kahn CR.** The insulin receptor in vertebrates is functionally more conserved during evolution than insulin itself. *Endocrinology*. 1979; 104(5):1393–1402.
10. **White MF.** The insulin signalling system and the IRS proteins. *Diabetologia*. 1997;40(suppl 2):S2–S17.
11. **Fafalios A, Ma JH, Tan XP, et al.** A hepatocyte growth factor receptor (Met)-insulin receptor hybrid governs hepatic glucose metabolism. *Nat Med*. 2011;17(12):U1577–U1587.
12. **Claeys I, Simonet G, Poels J, et al.** Insulin-related peptides and their conserved signal transduction pathway. *Peptides*. 2002;23(4):807–816.
13. **Hubbard SR.** The insulin receptor: Both a prototypical and atypical receptor tyrosine kinase. *Cold Spring Harb Perspect Biol*. 2013; 5(3):a008946.
14. **Nef S, Verma-Kurvari S, Merenmies J, et al.** Testis determination requires insulin receptor family function in mice. *Nature*. 2003; 426(6964):291–295.
15. **Chandler JC, Aizen J, Elizur A, Hollander-Cohen L, Battaglene S, Ventura T.** Discovery of a novel insulin-like peptide and insulin binding proteins in the Eastern rock lobster, *Sagmariasus verreauxi*. *Gen Comp Endocrinol*. 2015;215:76–87.
16. **Ventura T, Manor R, Aflalo ED, Weil S, Rosen O, Sagi A.** Timing sexual differentiation: full functional sex reversal achieved through silencing of a single insulin-like gene in the prawn, *Macrobrachium rosenbergii*. *Biol Reprod*. 2012;86(3):90, 91–96.
17. **Ventura T, Manor R, Aflalo ED, Chalifa-Caspi V, Weil S, Sharabi O, Sagi A.** Post-embryonic transcriptomes of the prawn *Macrobrachium rosenbergii*: multigenic succession through metamorphosis. *PLoS One*. 2013;8(1):e55322.
18. **Jung H, Lyons RE, Dinh H, Hurwood DA, McWilliam S, Mather PB.** Transcriptomics of a giant freshwater prawn (*Macrobrachium rosenbergii*): de novo assembly, annotation and marker discovery. *PLoS One*. 2011;6(12):e27938.
19. **Schultz J, Milpetz F, Bork P, Ponting CP.** SMART, a simple modular architecture research tool: identification of signaling domains. *Proc Natl Acad Sci USA*. 1998;95(11):5857–5864.
20. **Sievers F, Wilm A, Dineen D, et al.** Fast, scalable generation of high-quality protein multiple sequence alignments using Clustal Omega. *Mol Syst Biol*. 2011;7:539.
21. **Sievers F, Higgins DG.** Clustal omega. *Curr Protoc Bioinformatics*. 2014;48:3.13.1–3.13.16.
22. **Dobin A, Davis CA, Schlesinger F, et al.** STAR: ultrafast universal RNA-seq aligner. *Bioinformatics*. 2013;29(1):15–21.
23. **Sharabi O, Ventura T, Manor R, Aflalo ED, Sagi A.** Epidermal growth factor receptor in the prawn *Macrobrachium rosenbergii*: function and putative signaling cascade. *Endocrinology*. 2013; 154(9):3188–3196.
24. **Vázquez-Islas G, Guerrero-Tortolero DA, Garza-Torres R, Álvarez-Ruiz P, Mejía-Ruiz H, Campos-Ramos R.** Quantitative analysis of hypertrophy and hyperactivity in the androgenic gland of eyestalk-ablated male Pacific white shrimp *Litopenaeus vannamei* during molt stages. *Aquaculture*. 2015;439(0):7–13.
25. **Ventura T, Sagi A.** The insulin-like androgenic gland hormone in crustaceans: from a single gene silencing to a wide array of sexual manipulation-based biotechnologies. *Biotechnol Adv*. 2012;30(6): 1543–1550.
26. **Maori E, Paldi N, Shafir S, et al.** IAPV, a bee-affecting virus associated with colony collapse disorder can be silenced by dsRNA ingestion. *Insect Mol Biol*. 2009;18(1):55–60.
27. **Lezer Y, Aflalo ED, Manor R, Sharabi O, Abilevich LK, Sagi A.** On the safety of RNAi usage in aquaculture: The case of all-male prawn stocks generated through manipulation of the insulin-like androgenic gland hormone. *Aquaculture*. 2015;435:157–166.
28. **Cohen D, Raanan Z, Brody T.** Population profile development and morphotypic differentiation in the giant freshwater prawn *Macrobrachium rosenbergii* (de man). *J World Maricult Soc*. 1981;12(2): 231–243.
29. **Cohen D, Ra'anan Z, Rappaport U, Arieli Y.** The production of the freshwater prawn *Macrobrachium rosenbergii* (De Man) in Israel: improved conditions for intensive monoculture. *Bamidgeh*. 1983; 35:31–37.
30. **Nagamine CM, Knight AW.** Development, maturation, and function of some sexually dimorphic structures of the Malaysian prawn,

Macrobrachium Rosenbergii (De Man) (*Decapoda, Palaemonidae*). *Crustaceana*. 1980;39(2):141–152.
31. **Aizen J, Kasuto H, Golan M, Zakay H, Levavi-Sivan B.** Tilapia follicle-stimulating hormone (FSH): immunochemistry, stimulation by gonadotropin-releasing hormone, and effect of biologically active recombinant FSH on steroid secretion. *Biol Reprod*. 2007; 76(4):692–700.
32. **Roth Z, Khalaila I.** Identification and characterization of the vitellogenin receptor in *Macrobrachium rosenbergii* and its expression during vitellogenesis. *Mol Reprod Dev*. 2012;79(7):478–487.
33. **Escobar S, Fuentes EN, Poblete E, et al.** Molecular cloning of IGF-1 and IGF-1 receptor and their expression pattern in the Chilean flounder (*Paralichthys adspersus*). *Comp Biochem Physiol B Biochem Mol Biol*. 2011;159(3):140–147.
34. **Wheeler DE, Buck N, Evans JD.** Expression of insulin pathway genes during the period of caste determination in the honey bee, *Apis mellifera*. *Insect Mol Biol*. 2006;15(5):597–602.
35. **Kimura KD, Tissenbaum HA, Liu YX, Ruvkun G.** daf-2, an insulin receptor-like gene that regulates longevity and diapause in *Caenorhabditis elegans*. *Science*. 1997;277(5328):942–946.
36. **Ventura T, Rosen O, Sagi A.** From the discovery of the crustacean androgenic gland to the insulin-like hormone in six decades. *Gen Comp Endocrinol*. 2011;173(3):381–388.
37. **Chan SJ, Steiner DF.** Insulin through the ages: phylogeny of a growth promoting and metabolic regulatory hormone. *Am Zool*. 2000; 40(2):213–222.
38. **Martin JA, Wang Z.** Next-generation transcriptome assembly. *Nat Rev Genet*. 2011;12(10):671–682.
39. **Marguerat S, Bahler J.** RNA-seq: from technology to biology. *Cell Mol Life Sci*. 2010;67(4):569–579.
40. **Boucher P, Ditlecadet D, Dube C, Dufresne F.** Unusual duplication of the insulin-like receptor in the crustacean *Daphnia pulex*. *BMC Evol Biol*. 2010;10:305.
41. **Sroyraya M, Chotwiwatthanakun C, Stewart MJ, et al.** Bilateral eyestalk ablation of the blue swimmer crab, *Portunus pelagicus*, produces hypertrophy of the androgenic gland and an increase of cells producing insulin-like androgenic gland hormone. *Tissue Cell*. 2010;42(5):293–300.
42. **Apweiler R, Hermjakob H, Sharon N.** On the frequency of protein glycosylation, as deduced from analysis of the SWISS-PROT database. *Bba-Gen Subjects*. 1999;1473(1):4–8.
43. **Varki A.** Biological roles of oligosaccharides—all of the theories are correct. *Glycobiology*. 1993;3(2):97–130.
44. **Elleman TC, Frenkel MJ, Hoyne PA, et al.** Mutational analysis of the N-linked glycosylation sites of the human insulin receptor. *Biochem J*. 2000;347:771–779.
45. **Leevers SJ.** Growth control: invertebrate insulin surprises! *Curr Biol*. 2001;11(6):R209–R212.
46. **Chiu SL, Cline HT.** Insulin receptor signaling in the development of neuronal structure and function. *Neural Dev*. 2010;5.
47. **Bateman JM, McNeill H.** Temporal control of differentiation by the insulin receptor/tor pathway in Drosophila. *Cell*. 2004;119(1):87–96.
48. **Tatar M, Kopelman A, Epstein D, Tu MP, Yin CM, Garofalo RS.** A mutant Drosophila insulin receptor homolog that extends life-span and impairs neuroendocrine function. *Science*. 2001;292(5514):107–110.
49. **Chen C, Jack J, Garofalo RS.** The Drosophila insulin receptor is required for normal growth. *Endocrinology*. 1996;137(3):846–856.
50. **Steele RE, Lieu P, Mai NH, Shenk MA, Sarras MP Jr.** Response to insulin and the expression pattern of a gene encoding an insulin receptor homologue suggest a role for an insulin-like molecule in regulating growth and patterning in Hydra. *Dev Genes Evol*. 1996; 206(4):247–259.
51. **Alfaro J, Ulate K, Vargas M.** Sperm maturation and capacitation in the open thelycum shrimp Litopenaeus (Crustacea: Decapoda: Penaeoidea). *Aquaculture*. 2007;270(1–4):436–442.
52. **Khalaila I, Manor R, Weil S, Granot Y, Keller R, Sagi A.** The eyestalk-androgenic gland-testis endocrine axis in the crayfish Cherax quadricarinatus. *Gen Comp Endocrinol*. 2002;127(2):147–156.